An Efficient Nypa Fiber Waste Conversion to Activated Carbon for Li-ion Battery Anode Material

Cornelius Satria Yudha
Department of Chemical Engineering, UNS Vocational School, Universitas Sebelas Maret

Anjas Prasetya Hutama
Department of Chemical Engineering, UNS Vocational School, Universitas Sebelas Maret

Himmah Sekar Eka Ayu Gustiana
Department of Chemical Engineering, UNS Vocational School, Universitas Sebelas Maret

Windhu Griyasti Suci
Department of Chemical Engineering, UNS Vocational School, Universitas Sebelas Maret

他

https://doi.org/10.5109/7236863

出版情報：Evergreen. 11 (3), pp.2193-2201, 2024-09. 九州大学グリーンテクノロジー研究教育センター
バージョン：

An Efficient Nypa Fiber Waste Conversion to Activated Carbon for Li-ion Battery Anode Material

Cornelius Satria Yudha[1,2,*], Anjas Prasetya Hutama[1,2], Himmah Sekar Eka Ayu Gustiana[1,2], Windhu Griyasti Suci[1,2], Muhammad Iqbal Al-Fuady[1,2]

[1]Department of Chemical Engineering, UNS Vocational School, Universitas Sebelas Maret, Jl. Kolonel Sutarto 150K, Surakarta, Indonesia, 571262

[2]Centre of Excellence for Electrical Energy Storage Technology, Universitas Sebelas Maret

*Author to whom correspondence should be addressed:
E-mail: corneliussyudha@staff.uns.ac.id

(Received October 29, 2023: Revised June 8, 2024: Accepted June 21, 2024).

Abstract: Functional carbon derived from biomass waste has a high potential to be adapted as an active anode material for energy storage technology. *Nypa fruticans* or nypa plantations aim to avoid abrasion and generate biomass waste such as fibers. In this research, we report the utilization of activated carbon derived from Nypa fiber (ACNF) for $LiNi_{0.6}Co_{0.2}Mn_{0.2}O_2$ batteries. An efficient single-step pyrolysis and chemical activation process achieved the activated carbon. Cheap and commercially available KOH, H_3PO_4, and K_2CO_3 were the activating agents. The effect of activating agents on the characteristics of ACNF was deeply investigated. X-ray diffraction, FTIR, SEM-EDX, TG-DTA, and N_2 isotherms analyses were performed. XRD, FTIR, and SEM-EDX analysis confirm high carbon content samples. SEM images presented porous particles, while surface area analysis using the BET method shows that all samples have mesoporous pore size and surface area larger than 850 m^2/g. Charge discharge analysis in cylindrical-type cells shows the highest capacity of 89.5 mAh/g_{NCM}, established with KOH activation and an initial coulombic efficiency of 53.2%. Ultimately, Nypa fiber-derived activated carbon is successfully obtained and utilized in a state-of-the-art Li-ion battery cell with promising results.

Keywords: Activated carbon; anode material; batteries; Li-ion battery; Waste

1. Introduction

Nypa (*Nypa fruticans*) is one of the main species that make up mangrove forests; it belongs to the Palmae family, grows in tidal areas, and is spread almost evenly throughout Indonesia, specifically the islands of Sumatra, Java, Borneo, Sulawesi, Maluku, and Irian Jaya. Nypa plantations are needed in coastal areas to prevent abrasion. On the other hand, the Nypa palm tree can produce fruit weighing approximately 5 kg/tree and produce biomass waste of roughly 3 kg, mainly in the form of its shells/fibers. The fibers of the Nypa fruit are rarely used, so they are often thrown away and become waste. Nypa fibers contain high lignocellulosic elements, reaching 87.1%, which is suitable as a source for carbon-based materials[1,2)].

Activated carbon (AC) is a porous solid containing 80-95% carbon produced from carbon-rich sources that undergo activation. The activation process causes pore formation, increasing its surface area, which is suitable for numerous applications such as waste treatments and energy storage applications[3,4)]. Activated carbon is often used as an additive for Li-ion battery materials[5–8)]. It is often used to improve the conductivity of cathodes and anode materials. Recent studies confirm the successful application of AC as an anode material for Li-ion batteries to substitute graphite, which has been used commercially. Artificial graphite is currently the most often used as an anode (theoretical capacity of 372 $mAhg^{-1}$)[9)]. However, the formation of graphite requires a high amount of energy due to the graphitization of carbon reaching a temperature of 2800 °C; thus, it can be considered uneconomical and not eco-friendly. Various researchers have reported different types of carbons derived from biomass such as corncobs, rice husk, coconut shells and fibers, palms, bamboo, and sawdust to improve the performance, cost, efficiency, and eco-friendliness of the anode material[10–13)]. Nypa fiber-based activated carbon has reportedly been applied as a supercapacitor with specific capacitance values of 320, 430, 387 Fg^{-1} [14)] and 186, 214, 163 Fg^{-1} [15)]. Based on these findings, developing LIBs anode material derived from Nypa is highly promising. Herein, this

research reported the synthesis of activated carbon (AC) from Nypa fruit fibers to be applied as anode material for Li-ion batteries' full cells. A single-step co-carbonization-chemical activation method was performed, and the KOH, K_2CO_3, and H_3PO_4 were utilized as the chemical activators. The KOH, K_2CO_3, and H_3PO_4 represent basic, salt-based, and acidic chemical activators, respectively, that are well known for their mild properties and safety, compared to heavy metals-based chemical activators such as $FeCl_3$ or $ZnCl_2$[16]. The single-step technique was used instead of the subsequent carbonization-activation process to reduce the overall processing time and to avoid an extremely large surface area due to its tendency to form solid-electrolyte interphase (SEI), which severe the electrochemical performance of carbon-based anode during the charge-discharge process such as large irreversible capacity and impedance[17,18]. This research also explored extensive characterization studies of the as-prepared activated carbon to provide a thorough and deep discussion. The overall synthesis process can be considered cost, energy-, time-saving, efficient, and simple, which will be beneficial when applied on an industrial scale. The result of the electrochemical performance analysis in a full cell provides evidence for the successful and direct implementation of the anode material in a commercial cell.

2. Materials and Methods

Nypa (*Nypa fruticans)* fibers were converted to activated carbon through simultaneous activation and carbonization. This process requires a shorter time, and it will be more economical and practical. Nypa fibers were obtained from Pangandaran Regency, West Java, Indonesia. The fibers were obtained by separating the shell/husk and the fruit, followed by the chopping process using sharp cutters such as wire nippers. The chemical activating agents (KOH, H_3PO_4, and K_2CO_3) were obtained from Merck, Germany. The Nypa fruit fiber was dried, ground, and mashed into powder. Then, the Nypa fibers were submerged in solutions containing 5% w/w of KOH, K_2CO_3, and H_3PO_4, respectively. The Nypa fibers: activating agent mass ratio is 1:1. The impregnation of activating agents to the Nypa fibers was 24 hours. The Nypa powder was then filtered and dried, followed by a calcination/carbonization process at 650 C for 150 minutes to obtain crude activated carbon powder. The crude-activated carbon powder was washed multiple times using distilled water and ethanol. The as-described process is depicted in Fig. 1. The samples were labeled ACNF-KOH, ACNF-H_3PO_4, and ACNF-K_2CO_3, corresponding to the activating agents.

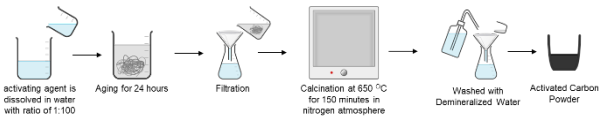

Fig. 1: Synthesis of Activated Carbon from Nypa Fibers (ACNF) by Chemical Activation Method

The structural and crystal property of the activated carbon powder was examined using an X-ray diffractometer (mini diffractometer MD-10) at a diffraction angle of 15 - 65 ° and a CuKα- wavelength of 1.5418 Å. SEM (Scanning electron microscopy, JEOL Japan) investigation was conducted to evaluate the morphological features of the ACNFs. Fourier Transform Infra-Red (Shimadzu IR-Spirit, Japan) was used to evaluate the functional groups contained in the samples. A thermogravimetric analysis was conducted to study the chemical activation process of Nypa fiber coupled with differential thermal analyses (TG/DTA, Shimadzu DTG-60 Japan). Quantachrome Instruments (Quantachrome Ins, USA) investigated the surface area and pore dimensions.

ACNF samples were applied as the lithium-ion batteries' active anode material. $LiNi_{0.6}Co_{0.2}Mn_{0.2}O_2$ or NCM-622 was utilized as the counter electrode. ACNF and NCM-622 sheets were prepared by dissolving the active material (AM) powder, carbon black powder, carboxy methyl cellulose (CMC) binder, and styrene butadiene rubber (SBR) with a weight ratio of 70: 15: 5: 10 in demineralized water to form a slurry. The slurry was then coated on both sides of the current collector foils, followed by drying under vacuum at 90 °C. Al and Cu foils were used as positive and negative current collectors, respectively. The assembly of cylindrical cells and electrolyte filling process of 18650-type cylindrical LIBs were explained in our previous studies[19,20]. The battery cells were tested in the voltage window, and the current rate was 2.4-4.3 V and 1/10 C under room conditions using a Battery Analyzer (Arbin Instruments, USA).

3. Results and Discussions

This section intensely studied the effect of chemical activating agents on the characteristics of the ACNF.

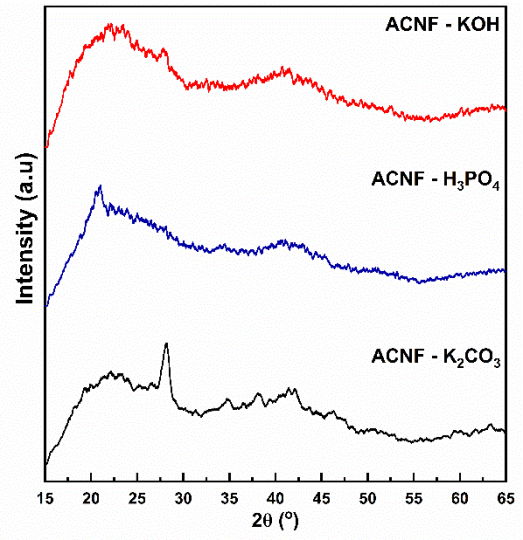

(a)

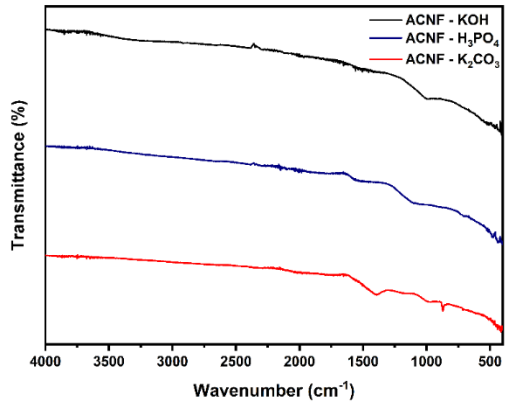

(b)

Fig. 2: (a) XRD Pattern and (b) FTIR spectra of ACNF with various activating agents

The diffraction pattern of activated carbon derived from Nypa fiber (ACNF) activated using KOH, H_3PO_4, and K_2CO_3 is shown in Fig. 2(a). These chemical activating agents were chosen due to their availability, safety, and economic aspects compared to other transitional metal-based activating agents such as $ZnCl_2$, $FeCl_3$, Fe-Citrate, and strong acids such as H_2SO_4 and HCl as reported in previous studies[21]. KOH, H_3PO_4, and K_2CO_3 are considered cheap, eco-friendly, and abundant.[22] Based on the figure, all samples have a semicrystalline carbon phase with low diffraction intensity, similar to previous studies[23–25]. All of the samples exhibit typical characteristics of amorphous carbon where broad peaks are clearly observed at diffraction angles of 22° and 40° (JCPDF Card, No.04– 018-7559). However, there are significant peaks of crystalline graphite in the ACNF-K_2CO_3 sample, specifically at a diffraction angle of 26°, 36°, and 41°. The formation of graphite during the activation of biomass by K_2CO_3 is also found in the research conducted by Xi *et al.* [26] and Purwanto *et. al*[27], which confirms that during the heat treatment, K_2CO_3 turns into K_2O then followed by the formation of reduced K which allows local ordering of carbon structure thus increasing the graphitization of carbon. This phenomenon also cannot be found in samples activated by KOH and H_3PO_4. The formation of carbon material is also confirmed by the FTIR spectroscopy analysis results displayed in Fig. 2(b). A peak was formed around 1500 cm^{-1} (C=O) and also around 1200 cm^{-1} (C-O), this result is similar to the research of Ridassepri *et. al*[28]and Wang *et. al*[29] The transmission peaks are only slightly observable at 1000 cm^{-1} -1400 cm^{-1} wavenumber, which can be attributed to low C-O or carboxylic group content in the sample.[25] No hydroxyl peak means the carbonization and activation resulting to enlargement area of sample with low level of organic impurities are successfully conducted.

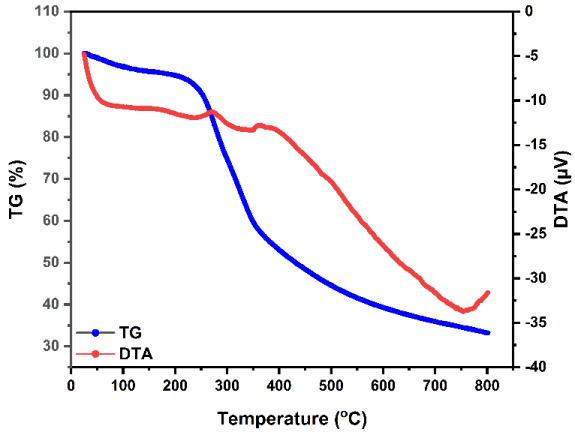

(a)

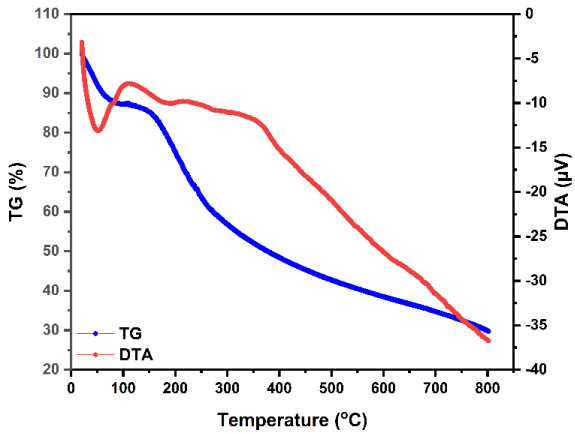

(b)

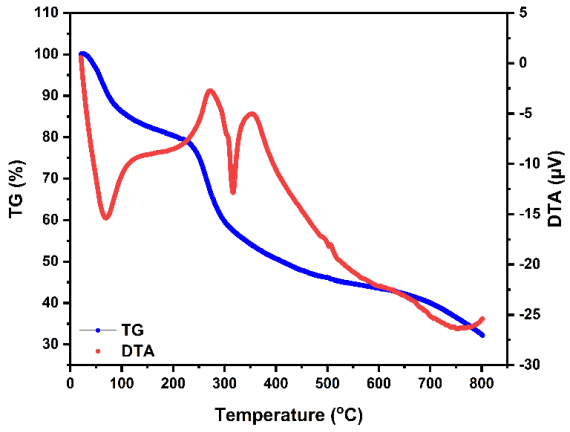

(c)

Fig. 3: TG/DTA analysis of Nypa fiber chemical activation using (a) KOH, (b) H_3PO4, and (c) K_2CO_3

Nypa fiber's calcination process and chemical activation of Nypa fiber were investigated using differential thermal analysis/thermal gravimetry. The TG/DTA curve is displayed in Fig. 3. The weight losses are almost similar between each sample. The mass retention after being heated to 800 C under an N_2 atmosphere using KOH, H_3PO_4, and K_2CO_3 as chemical activating agents is 32.4%, 31.3%, and 33.4%, respectively. Since the Nypa fibers were not pre-carbonized, we can see that the decomposition of organic substance occurred gradually after the temperature reached 180 °C[30] Mass decrease before 180 °C can be attributed to the dehydration process of Nypa fiber, which is also confirmed by the presence of an endothermic peak. The decomposition peak can be clearly observed in K_2CO_3 activation; however, all samples undergo a similar pyrolysis process indicated by decreasing DTA curves starting from ~400 °C[31]. Miyajima *et al.*[32] *and Liu et al. reported a similar thermogravimetric analysis of chitosan-based carbon activation using K2CO3, revealing the presence of decomposition of organic material indicated by a* significant DTA curve.

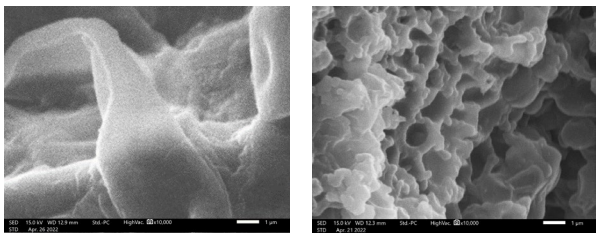

(a) (b)

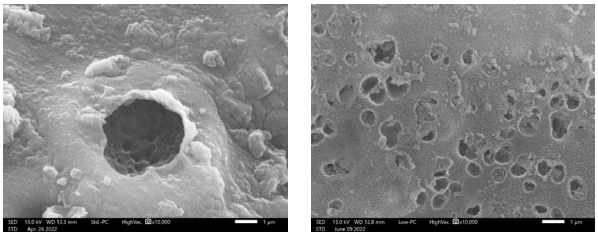

(c) (d)

Fig. 4: SEM Images of (a) pre-treated nypa fibers, (b) ACNF-KOH, (c) ACNF-H_3PO_4, and (d) ACNF-K_2CO_3

SEM characterization was conducted to determine activated carbon's morphological features and characteristics. In addition, this test to determine the presence of pores formed in the sample. Figure 4 displays the SEM images of untreated Nypa fibers, and ACNF activated using KOH, H_3PO_4, and K_2CO_3. It can be clearly observed that large pores are formed after pyrolytic decomposition at high temperatures. It also can be seen, especially in ACNF-H_3PO_4 and ACNF-K_2CO_3, that small-sized pores can be directly seen. The presence of pores indicates a significant increase in the surface area of activated carbon. The particle size is less than 32 micrometers. The EDX analysis of Nypa fiber and ACNF samples can be seen in Table 2. The dominant elements appear during analysis are C and O[32], the significant amount of O in Nypa fiber is normal due to its composition consisting lignocellulosic or hydrocarbon compounds[33]. Conversely, a high level of C can be seen in ACNF samples with a nonnegligible amount of O atom. Since the FTIR studies show a low level of the carboxylic group, it can be concluded that the presence of O only appears on the surface of the ACNF particle. Meanwhile, the samples are considered to have a high amount of carbon.

Table 1. EDX Analysis of Activated Carbon with Various Activators

Element	Sample							
	Nypa Fiber		ACNF-KOH		ACNF-H_3PO_4		ACNF-K_3CO3	
	w%	mole %	w%	mole %	w%	mole %	w%	mole %
C	39.27	48.16	73.42	80.97	71.57	78.95	71.19	78.34
O	52.05	47.87	20.05	16.58	22.33	18.47	23.70	19.56
Na	1.54	0.98	0.69	0.40	-	-	-	-
Al	1.02	0.56	-	-	0.81	0.40	0.51	0.25
Cl	3.16	1.31	-	-	-	-	-	-
K	2.12	0.81	3.50	1.18	-	-	-	-
Ca	0.84	0.31	1.72	0.57	0.73	0.24	2.18	0.71
Si	-	-	0.63	0.30	-	-	2.41	1.14
P	-	-	-	-	4.55	1.94	-	-

The size of the pores can be evaluated by N_2 isotherm adsorption and measured using the BET method. The result of the size analysis can be seen in Fig. 5.

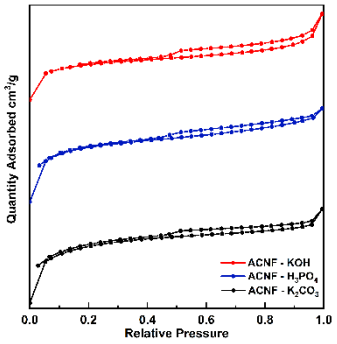

(a)

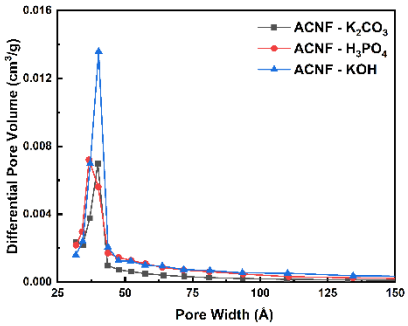

(b)

Fig. 5: (a) N2 Adsorption–desorption Isotherms and (b) DFT Pore Size Distributions for AC with Different Activating Agents

Figure 5 presents adsorption-desorption isotherms of N_2 and DFT pore size distributions of ACNF samples. These isotherms curves from Fig. 5 (a) seemed to be Type II adsorption, meaning all the samples have micro and mesopores. Above 0.4 relative pressure, the isotherms demonstrate hysteresis Type H4 loops.[34] Figure 2 confirms the presence of mesopores in all samples. The mesopores not only improve the Li-ion storage capacity but also improve material conductivity. The pore and area measurements analysis result can be seen in Table 2. The largest surface area is achieved by K_2CO_3 activation. We can predict that the activation processes undergo steps of reactions. The KOH activation reaction can be seen in the following equations:

$$C_{(s)} + 3KOH_{(s)} \rightarrow K_{(s)} + 3/2\ H_{2(g)} + K_2CO_{3(s)} \quad (1)$$
$$K_2CO_{3(s)} \rightarrow K_2O_{(s)} + CO_{2(g)} \quad (2)$$
$$CO_{2(g)} + C_{(s)} \rightarrow CO_{(g)} \quad (3)$$
$$K_2O_{(s)} + C_{(s)} \rightarrow 2K_{(s)} + CO_{(g)} \quad (4)$$

When K_2CO_3 was used as an activating agent, reaction (1) was skipped, and the reaction is predicted in the following reaction:

$$K_2CO_{3(s)} + 2C_{(s)} \rightarrow 2K_{(s)} + 3CO_{(g)} \quad (5)$$

While in H_3PO_4 activation, the reaction can be explained in the following reaction:

$$2H_3PO_{4(l)} \rightarrow P_2O_{5(s)} + 3H_2O_{(g)} \quad (6)$$
$$2P_2O_{5(s)} + 5C_{(s)} \rightarrow 4P_{(s)} + 5CO_{2(g)} \quad (7)$$

The reactions confirm the mechanism of meso-micro pores formation. ACNF-K_2CO_3 has the highest surface area, which might result from an effective response in serial order compared to the KOH and H_3PO_4 activating agents. The lowest surface area and total of the pore volume is achieved by H_3PO_4 activation[21].

Table 2. Surface area analysis of ACNF samples

Samples	S_{BET} (m^2/g)	Average Pore Diameter (nm)	Total Pore Volume (cm^3/g)
ACNF-KOH	933.066	31.014	0.723
ACNF-H_3PO_4	856.218	25.805	0.552
ACNF-K_2CO_3	962.784	25.056	0.603

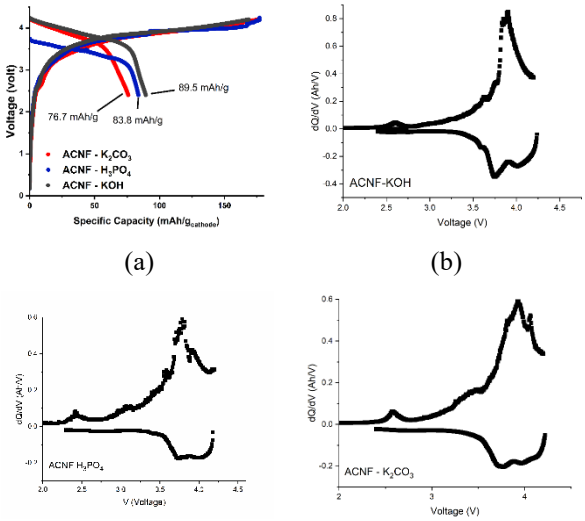

(a) (b)

(c) (d)

Fig. 6: (a) Charge – Discharge Analysis of ACNFs anode in Li-ion batteries cell and (b-d) dQ/dV vs V curve

Figure 6 shows the electrochemical performance of AC from various activating agents. An electrochemical performance test was carried out in a cylindrical cell and analyzed by evaluating the capacity of the cell where AC and NMC622 were applied as an anode and a cathode, respectively. The sample is tested by charging up to a voltage of 4.3 V. Then the battery sample is discharged until the voltage drops to 2.4 V, and the current used in this test is 0.1 C (1C=200 mA/$g_{cathode}$). The NMC 622 was selected as the limiting cathode electrode and the weight basis of capacity calculation with an estimated N/P ratio of 1.2-1.23).

Table 3. Charge-discharge analysis result of ACNF samples

Sample	Initial Specific Discharge Capacity	Initial Coulombic Efficiency	Initial Specific Discharge Energy	Initial Specific Discharge Power
ACNF-KOH	89.5 mAh/g_{NMC}	53.2 %	332 mWh/g_{NMC}	37.1 mW/g_{NMC}
ACNF-H_3PO4	83.8 mAh/g_{NMC}	47.0 %	322 mWh/g_{NMC}	38.7 mW/g_{NMC}
ACNF-K_2CO_3	76.7 mAh/g_{NMC}	43.1 %	284 mWh/g_{NMC}	37.7 mW/g_{NMC}

The specific discharge capacity of ACNF-KOH, ACNF-H_3PO_4, and ACNF-K_2CO_3, the initial coulombic efficiency (ICE), specific discharge energy and specific discharge power can be seen in Table 3. ACNF-KOH has the highest discharge capacity, energy and ICE, while the lowest discharge capacity and ICE are achieved by ACNF K_2CO_3. We can conclude that low ICE and capacity result from large surface area and small pore volume[35–37]. Large surface area can promote SEI, which leads to poor discharge capacity and irreversible Li-ion storage. The dQ/dV curve of ACNF samples shows that the SEI formation occurred at 2.5-2.7 V. The anodic peaks between 3.4-3.8 V indicate the carbon matrices' lithiation process. In all samples, the anodic peaks have a larger area than the cathodic peaks, which confirms the SEI formation of the ACNFs. This phenomenon can be seen clearly in ACNF-H_3PO_4. This phenomenon might be caused by a small pore volume in the sample, which promotes the occurrence of excess SEI and reduces the discharge capacity. Previous reports have often reported significant capacity loss during initial cycles. The comparative data from previous reports can be seen in Table 4. The loss of capacity in full-cell applications severs further utilization of ACs as anode materials[38,39]. Many researchers overcome this problem through the pre-lithiation process of the carbon electrode in a half-cell analysis[40,41]. This approach is considered not feasible for the industrial process. Based on our approach, the capacity loss in the initial cycle is less than 50%, which is an improvement. Synthesizing activated carbon with a lower surface area can improve the ICE. As shown in Table 2, ACs with large surface areas have the disadvantage of poor reversibility. Future studies in surface-area tuning must be developed to prevent capacity loss in full-cell batteries using simple methods.

Table 4. Comparison of Biomass-derived carbon's electrochemical performances as Li-ion anode

Biomass or Other source	Method	Initial Capacity (mAh/g)	ICE (%)	Ref
Bagasse	Hydrothermal	2347.56	50.55	42)
Tamarind Seeds	Chemical Activation using KOH	1037	39.93	43)
Rice Straw	Chemical Activation using KOH	2041	48.31	44)
Jute Fiber	Carbonization	1173.3	45.52	45)
Cherry Pit	Chemical Activation using KOH and H_3PO_4	1300	23.08	40)
Petroleum Coke	Catalytic conversion	100*	ND	46)
Nypa Fiber*	Chemical Activation using KOH	89.5*	53%	This work

*capacity of cathode (NCM) measured in full cell analysis

4. Conclusion

Activated carbons synthesized from *Nypa fruticans* fiber using various activating agents, i.e., KOH, H_3PO_4, and K_2CO_3, are successfully synthesized. The activated carbon can be used as an active material for energy storage, specifically Li-ion batteries using $LiNi_{0.6}Co_{0.2}Mn_{0.2}O_2$ as the cathode material. The XRD analysis result proved the presence of amorphous carbon. The FTIR analysis did not show a significant carboxylic group, indicating that the activated carbon samples have high carbon content, which was further proved by the SEM-EDX result. Based on the morphology and surface area analyses, it was found that there are nano-sized pores on activated carbon particles, indicating that the activated carbons have a high surface area and the activated carbon sample has a uniform particle pore size. The highest capacity is obtained by activated carbon with a KOH activation capacity of 89.5 mAh/g with a charge-discharge efficiency of 53.2%. The dQ/dV curve showed that the initial capacity loss was the result of SEI formation during the charging process. Further investigation on cycle-ability and rate-ability is promising and will be applied in future projects.

Acknowledgements

We are grateful for the financial support from Lembaga Penelitian dan Pengabdian Masyarakat (LPPM) Universitas Sebelas Maret through Penelitian Unggulan Terapan Scheme with contract number 194.2/UN27.22/PT.01.03/2024. We also acknowledge Meidiana Arinawati and Enni Apriliyani for the assistance during the research.

References

1) P. Tamunaidu, and S. Saka, "Chemical characterization of various parts of nipa palm (nypa fruticans)," *Ind Crops Prod*, **34** (*3*) 1423–1428 (2011). doi:10.1016/j.indcrop.2011.04.020.
2) B. Irawan, J. Khabibi, and A. Agustina, "The potential of nipah (nypa fruticans wurmb) as bioenergy

resources," *The 1st International Conference on Green Development – University of Jambi - 2016*, 83–86 (2016).
3) M.A. Tadda, A. Ahsan, A. Shifu, M. ElSergany, T. Arunkumar, B. Jose, M. Razzaque, Abdur, and N.N. Daud, Nik, "A review on activated carbon from biowaste : process , application and prospects," *Journal of Advanced Civil Engineering Practice and Research*, **5** (*3*) 82–83 (2018).
4) I. Syauqiah, M. Elma, D.P. Mailani, and N. Pratiwi, "Activated carbon from nypa (nypa fruticans) leaves applied for the fe and mn removal," *IOP Conf Ser Mater Sci Eng*, **980** (*1*) 1–8 (2020). doi:10.1088/1757-899X/980/1/012073.
5) B.A. Mahmoud, A.A. Mirghni, K.O. Oyedotun, D. Momodu, O. Fasakin, and N. Manyala, "Synthesis of cobalt phosphate-graphene foam material via co-precipitation approach for a positive electrode of an asymmetric supercapacitors device," *J Alloys Compd*, **818** 153332 (2020). doi:10.1016/j.jallcom.2019.153332.
6) S. Dong, X. Wang, L. Shen, H. Li, J. Wang, P. Nie, J. Wang, and X. Zhang, "Trivalent ti self-doped li4ti5o12: a high-performance anode material for lithium-ion capacitors," *Journal of Electroanalytical Chemistry*, **757** 1–7 (2015). doi:10.1016/j.jelechem.2015.09.002.
7) S. Agarwal, F. Nekouei, H. Kargarzadeh, S. Nekouei, I. Tyagi, and V. Kumar Gupta, "Preparation of nickel hydroxide nanoplates modified activated carbon for malachite green removal from solutions: kinetic, thermodynamic, isotherm and antibacterial studies," *Process Safety and Environmental Protection*, **102** 85–97 (2016). doi:10.1016/j.psep.2016.02.011.
8) Y. Gao, Q. Yue, B. Gao, and A. Li, "Insight into activated carbon from different kinds of chemical activating agents: a review," *Science of the Total Environment*, **746** 141094 (2020). doi:10.1016/j.scitotenv.2020.141094.
9) N. Nitta, F. Wu, J.T. Lee, and G. Yushin, "Li-ion battery materials: present and future," *Materials Today*, **18** (*5*) 252–264 (2015). doi:10.1016/j.mattod.2014.10.040.
10) X. Peng, J. Fu, C. Zhang, J. Tao, L. Sun, and P.K. Chu, "Rice husk-derived activated carbon for li ion battery anode," **6** (*1*) 68–71 (2014). doi:10.1166/nnl.2013.1714.
11) W. Tian, L. Wang, K. Huo, and X. He, "Red phosphorus filled biomass carbon as high-capacity and long-life anode for sodium-ion batteries," *J Power Sources*, **430** (*December 2018*) 60–66 (2019). doi:10.1016/j.jpowsour.2019.04.086.
12) G. Zhang, Y. Chen, Y. Chen, and H. Guo, "Activated biomass carbon made from bamboo as electrode material for supercapacitors," *Mater Res Bull*, **102** (*June 2017*) 391–398 (2018). doi:10.1016/j.materresbull.2018.03.006.
13) M.A. Tadda, A. Ahsan, A. Shifu, M. ElSergany, T. Arunkumar, B. Jose, M. Razzaque, Abdur, and N.N. Daud, Nik, "A review on activated carbon from biowaste : process , application and prospects," *Journal of Advanced Civil Engineering Practice and Research*, **5** (*3*) 82–83 (2018).
14) R. Farma, I. Apriyani, Awitdrus, M. Deraman, E. Taer, R.N. Setiadi, and A.S. Rini, "Enhanced electrochemical performance of oxygen, nitrogen, and sulfur trial-doped nypa fruticans-based carbon nanofiber for high performance supercapacitors," *J Energy Storage*, **67** (*February*) 107611 (2023). doi:10.1016/j.est.2023.107611.
15) R. Farma, A.N.I. Lestari, and I. Apriyani, "Supercapacitor cell electrodes derived from nipah fruticans fruit coir biomass for energy storage applications using acidic and basic electrolytes," *J Phys Conf Ser*, **2049** (*1*) (2021). doi:10.1088/1742-6596/2049/1/012043.
16) N.D. Andini, Y. Prasetiyani, F. Al Mumtahinah, B. Astika, and C. Satria, "The conversion of sorghum (sorghum bicolor (l .) moench) stem waste into activated carbon by the pyrolysis method using zncl 2 activator," **7** (*2*) 107–115 (2023).
17) S.K. Heiskanen, J. Kim, and B.L. Lucht, "Generation and evolution of the solid electrolyte interphase of lithium-ion batteries," *Joule*, **3** (*10*) 2322–2333 (2019). doi:10.1016/j.joule.2019.08.018.
18) Y. Rangom, R.R. Gaddam, T.T. Duignan, and X.S. Zhao, "Improvement of hard carbon electrode performance by manipulating sei formation at high charging rates," *ACS Appl Mater Interfaces*, **11** (*38*) 34796–34804 (2019). doi:10.1021/acsami.9b07449.
19) C.S. Yudha, M. Rahmawati, A. Jumari, A.P. Hutama, and A. Purwanto, "Synthesis of Zinc Oxide (ZnO) from Zinc Based-Fertilizer as Potential and Low-Cost Anode Material for Lithium Ion Batteries," in: ACM International Conference Proceeding Series, Association for Computing Machinery, 2020: pp. 1–6. doi:10.1145/3429789.3429860.
20) C.S. Yudha, S.U. Muzayanha, H. Widiyandari, F. Iskandar, W. Sutopo, and A. Purwanto, "Synthesis of lini0.85co0.14al0.01o2 cathode material and its performance in an nca / graphite full-battery," *Energies (Basel)*, **12** (*10*) (2019). doi:doi:10.3390/en12101886.
21) Y. Gao, Q. Yue, B. Gao, and A. Li, "Insight into activated carbon from different kinds of chemical activating agents: a review," *Science of the Total Environment*, **746** 141094 (2020). doi:10.1016/j.scitotenv.2020.141094.
22) C. Farkas, J.M. Rezessy-Szabó, V.K. Gupta, D.H. Truong, L. Friedrich, J. Felföldi, and Q.D. Nguyen, "Microbial saccharification of wheat bran for bioethanol fermentation," *J Clean Prod*, **240** (2019). doi:10.1016/j.jclepro.2019.118269.
23) S. Mopoung, R. Sitthikhankaew, and N. Mingmoon,

"Preparation of anode material for lithium battery from activated carbon," *International Journal of Renewable Energy Development*, **10** (*1*) 91–96 (2021). doi:10.14710/ijred.2021.32997.

24) K. Yu, J. Li, H. Qi, and C. Liang, "High-capacity activated carbon anode material for lithium-ion batteries prepared from rice husk by a facile method," *Diam Relat Mater*, **86** (*April*) 139–145 (2018). doi:10.1016/j.diamond.2018.04.019.
25) A.F. Ridassepri, F. Rahmawati, K.R. Heliani, Chairunnisa, J. Miyawaki, and A.T. Wijayanta, "Activated carbon from bagasse and its application for water vapor adsorption," *Evergreen*, **7** (*3*) 409–416 (2020). doi:10.5109/4068621.
26) Y. Xi, Y. Wang, D. Yang, Z. zhang, W. Liu, Q. Li, and X. Qiu, "K2CO3 activation enhancing the graphitization of porous lignin carbon derived from enzymatic hydrolysis lignin for high performance lithium-ion storage," *J Alloys Compd*, **785** 706–714 (2019). doi:10.1016/j.jallcom.2019.01.039.
27) A. Purwanto, M. Diantoro, A. Subagio, W. Meevasana, E. Apriliyani, C.S. Yudha, and H. Widiyandari, "Using tea waste to produce a high-performance lithium-ion capacitor—bio-graphite/ li4ti5o12 (lto)," *Results in Engineering*, **22** (*March*) 102156 (2024). doi:10.1016/j.rineng.2024.102156.
28) A.F. Ridassepri, F. Rahmawati, K.R. Heliani, Chairunnisa, J. Miyawaki, and A.T. Wijayanta, "Activated carbon from bagasse and its application for water vapor adsorption," *Evergreen*, **7** (*3*) 409–416 (2020). doi:10.5109/4068621.
29) R.S. Wang, Y. Li, X.X. Shuai, R.H. Liang, J. Chen, and C.M. Liu, "Pectin/activated carbon-based porous microsphere for pb2+ adsorption: characterization and adsorption behaviour," *Polymers (Basel)*, **13** (*15*) (2021). doi:10.3390/polym13152453.
30) F. Taufany, M.J. Pasaribu, B.Y.S. Romaji, Y. Rahmawati, A. Altway, Susianto, S. Nurkhamidah, J.G. Anfias, Y. Mursidah, D. Fujanita, S. Yulianti, D. Rahmawati, and G. Stellarosari, "The synthesis of activated carbon from waste tyre as fuel cell catalyst support," *Evergreen*, **9** (*2*) 412–420 (2022). doi:10.5109/4794166.
31) Y. Xi, Y. Wang, D. Yang, Z. zhang, W. Liu, Q. Li, and X. Qiu, "K2CO3 activation enhancing the graphitization of porous lignin carbon derived from enzymatic hydrolysis lignin for high performance lithium-ion storage," *J Alloys Compd*, **785** 706–714 (2019). doi:10.1016/j.jallcom.2019.01.039.
32) J.A. Hidayat, and B. Sugiarto, "Characteristic, structure, and morphology of carbon deposit from biodiesel blend," *Evergreen*, **7** (*4*) 609–614 (2020). doi:10.5109/4150514.
33) P. Tamunaidu, and S. Saka, "Chemical characterization of various parts of nipa palm (nypa fruticans)," *Ind Crops Prod*, **34** (*3*) 1423–1428 (2011). doi:10.1016/j.indcrop.2011.04.020.
34) M.N. Aprilliani, "Synthesis of activated carbon-fe _ 3o _ 4 composite as gasoline adsorbent in gasoline-water mixture and its adsorption kinetics study," *Evergreen*, **9** (*3*) 701–710 (2022). doi:10.5109/4843101
35) D.P. Dubal, V.J. Fulari, and C.D. Lokhande, "Effect of morphology on supercapacitive properties of chemically grown β-ni(oh) 2 thin films," *Microporous and Mesoporous Materials*, **151** 511–516 (2012). doi:10.1016/j.micromeso.2011.08.034.
36) M.Y. Cheng, Y.S. Ye, T.M. Chiu, C.J. Pan, and B.J. Hwang, "Size effect of nickel oxide for lithium ion battery anode," *J Power Sources*, **253** 27–34 (2014). doi:10.1016/j.jpowsour.2013.12.037.
37) Y. Rangom, R.R. Gaddam, T.T. Duignan, and X.S. Zhao, "Improvement of hard carbon electrode performance by manipulating sei formation at high charging rates," *ACS Appl Mater Interfaces*, **11** (*38*) 34796–34804 (2019). doi:10.1021/acsami.9b07449.
38) Y. Han, X. Liu, and Z. Lu, "Systematic investigation of prelithiated sio2 particles for high-performance anodes in lithium-ion battery," *Applied Sciences (Switzerland)*, **8** (*8*) (2018). doi:10.3390/app8081245.
39) T. Chen, J. Wu, Q. Zhang, and X. Su, "Recent advancement of siox based anodes for lithium-ion batteries," *J Power Sources*, **363** 126–144 (2017). doi:10.1016/j.jpowsour.2017.07.073.
40) C. Hernández-Rentero, V. Marangon, M. Olivares-Marín, V. Gómez-Serrano, Á. Caballero, J. Morales, and J. Hassoun, "Alternative lithium-ion battery using biomass-derived carbons as environmentally sustainable anode," *J Colloid Interface Sci*, **573** 396–408 (2020). doi:10.1016/j.jcis.2020.03.092.
41) Y. Han, X. Liu, and Z. Lu, "Systematic investigation of prelithiated sio2 particles for high-performance anodes in lithium-ion battery," *Applied Sciences (Switzerland)*, **8** (*8*) (2018). doi:10.3390/app8081245.
42) S. Zheng, Y. Luo, K. Zhang, H. Liu, G. Hu, and A. Qin, "Nitrogen and phosphorus co-doped mesoporous carbon nanosheets derived from bagasse for lithium-ion batteries," *Mater Lett*, **290** (2021). doi:10.1016/j.matlet.2021.129459.
43) M.R. Panda, A.R. Kathribail, B. Modak, S. Sau, D.P. Dutta, and S. Mitra, "Electrochemical properties of biomass-derived carbon and its composite along with na2ti3o7 as potential high-performance anodes for na-ion and li-ion batteries," *Electrochim Acta*, **392** (2021). doi:10.1016/j.electacta.2021.139026.
44) F. Zhang, K.X. Wang, G.D. Li, and J.S. Chen, "Hierarchical porous carbon derived from rice straw for lithium ion batteries with high-rate performance," *Electrochem Commun*, **11** (*1*) 130–133 (2009). doi:10.1016/j.elecom.2008.10.041.
45) Y. Dou, X. Liu, X. Wang, K. Yu, and C. Liang, "Jute fiber based micro-mesoporous carbon: a biomass derived anode material with high-performance for lithium-ion batteries," *Materials Science and*

Engineering: B, **265** (2021). doi:10.1016/j.mseb.2020.115015.

46) A. Nugroho, E.B. Nursanto, S.A. Pradanawati, H.S. Oktaviano, H. Nilasary, and H. Nursukatmo, "Fe based catalysts for petroleum coke graphitization for lithium ion battery application," *Mater Lett*, **303** (2021). doi:10.1016/j.matlet.2021.130557.